Requirement Derivation of Vehicle Steering Using Mechanical Four-Poles

M. Muenster[a,*], M. Lehner[a], D. Rixen[b]

[a] *BMW Group, Development Driving Dynamics, Knorrstr. 147, D-80788, München, Germany*
[b] *Technische Universität München, Institute of Applied Mechanics, Boltzmannstr. 15, D-85748 Garching, Germany*

Abstract

Vehicle design with respect to steering feel and steering vibration is challenging for many reasons. One of them is that several subsystems need to be considered simultaneously, which are developed separately by different departments or external suppliers. Therefore, the requirements, which are usually imposed on the vehicle level, i. e. the coupled system, have to be reformulated on the level of subsystems. In this work, objective requirements on the steering subsystem are derived using mechanical four-poles. For this purpose, the vehicle system is divided into steering and front axle subsystems. Basic equations are derived in order to determine the relevant four-pole coefficients and to derive requirements to the subsystems by disassembling them from given vehicle system dynamics. Both virtual and experimental methods can be used to determine the relevant four-pole coefficients of the steering and the front axle during the design and verification stages. Vehicle targets are introduced, depending on vehicle speed or excitation frequency. Then, requirements in terms of necessary, sufficient and phase-exact limit values to selected subsystem dynamics are calculated. By assembling actual and permissible dynamics of the subsystems, the performance at vehicle level becomes predictable. It is shown that target mismatch can be detected already at subsystem level during the design phase, where corrective measures are still feasible. Reversely, vehicle targets are met if the subsystems fulfill their respective requirements.

Keywords: vehicle handling and comfort, steering gear, front axle, four-pole, frequency based substructuring, requirement derivation, subsystem dynamics, multi-body simulation, virtual roller-testrig, target cascading, robust design

1. Introduction

Substructuring methods have been used for many years in various industrial applications to simplify or even enable the calculation of dynamics of very large structures [1, 2]. The basic idea is the partitioning of the whole structure into smaller substructures which can be analyzed, measured or simulated more efficiently. Afterwards, the dynamics of the complete structure can be predicted easily by assembling the dynamics of all substructures. Common problems handled with substructuring methods are in the field of sound and vibration. But even mechatronic systems, such as electrical power steering, have been analyzed in recent years in terms of structure-born noise [3, 4, 5, 6]. Typically, substructuring methods are used to assemble all subsystems in order to predict the global dynamics with limited calculation effort, but still high accuracy. In other words, the main view using substructuring methods so far is rather bottom-up than top-down.

One of the first and simplest substructuring technique is the so-called four-pole method, which only uses input and output measures of the unknown structure or a black-box-system. Being originally designed for interconnected electrical circuits (where voltage and current at both the input and output ports constitute the four "poles"), it has been applied to acoustics as well as to mechanical systems [7, 8, 9, 10, 11, 12, 13].

*Corresponding author, Tel.: +49 89 382 45589
Email addresses: martin.muenster@bmw.de (M. Muenster), michael.la.lehner@bmw.de (M. Lehner), rixen@tum.de (D. Rixen)

The four-pole method is limited to strictly parallel or serial arrangements, i. e. not suitable for arbitrarily connected structures, but typically the complexity to build the transfer function for an assembly using substructure transfer information is very low. This is advantageous for top-down approaches, when only few targets in terms of desired properties of the coupled structure are given, which have to be split up into corresponding requirements for the dynamics of their subsystems and components.

In the case of vehicle steering design, when mechatronic or mechanical subsystems such as the electric power steering and the front suspension are being developed by different companies simultaneously, the desired steering feel after completion of the vehicle has to be expressed by cascaded requirements at the level of these subsystems. Although vehicle targets are available in the form of permissible amplitudes of vibration, allowed amplitudes of the subsystems depend on the specific interaction between them, which is not known in advance.

This paper presents an approach based on the four-pole method and allowing to apply substructuring to top-down vehicle steering design. As example, the problem of steering vibration will be considered. Unlike the majority of common substructuring problems, the main focus is set on the decoupling of the subsystems involved, where particularly the four-pole method seems to be favorable. It is not the intention to predict the dynamics of the global system with highest accuracy, but to derive requirements, which are useful in practice for the developers having access only to their respective subsystem. The requirements are based on defined vehicle targets who represent limitations to the vibration amplitudes of the coupled system after the vehicle is assembled with the steering. Finally, the expectable vehicle performance is predicted by assembling both actual and permissible dynamics of suspension and steering. It is shown that the vehicle targets are met if the subsystems fulfill their respective requirements derived from the four-pole method.

2. Substructuring Vehicle Steering System

Steering systems of vehicles establish a tactile connection between the driver's hands and the tire-road contact patch. On the one hand, the transmission of mechanical vibration by this connection is a desired contribution to the steering feel. Information on road characteristics and friction conditions of the tire helps the driver to control the vehicle. On the other hand, undesired vibrations are inevitably transmitted via this connection too. Due to wheel imperfections such as imbalance or stiffness variation, the rolling tire induces force variations which are propagated to the driver by the steering even if the road is perfectly smooth.

Both effects build up the disturbance response of a coupled system, which may be divided into subsystems such as the wheel, suspension, steering gear and upper steering column, for instance. Today, the disturbance response cannot be assessed until all subsystems are integrated into the vehicle. As a consequence, deviations of the desired behavior cannot be detected until subsystem development is almost finished, which is too late for solving vibrational problems efficiently. Appropriate methods, which are capable of ensuring the desired disturbance behavior of the vehicle, starting from the virtual development phase, are needed therefore. Objective requirements, given on a vehicle level, have to be split up into a set of corresponding criteria formulated on the level of subsystems or components.

2.1. Vehicle System and Subsystems Overview

The vehicle system, i. e. the coupled system analyzed in this paper, comprises the entire transmission path starting from the tire contact patch and ending at the steering wheel as interface to the driver, as shown in Fig. 1. To enhance visibility, the wheels, the suspension linkages and the left part of the front axle are hidden though being part of the system investigated. The system is subdivided into two subsystems, the front axle and the steering. Assuming that the conceptual layout of one of the subsystems is available already (or its design is shared with other vehicle models), one has to disconnect the known subsystem from the vehicle system to get requirements for the relevant dynamic properties of the unknown subsystem which are dictated by both the vehicle targets and the actual dynamics of the known subsystem.

As mechanical interface, the connection point of the steering rack to one of the tied rods is chosen. The steering rack is connected symmetrically to the right and left wheel of the front axle via tie rods and ball joints. Due to the fact that the rack moves as a rigid body along its longitudinal axis only and is driven

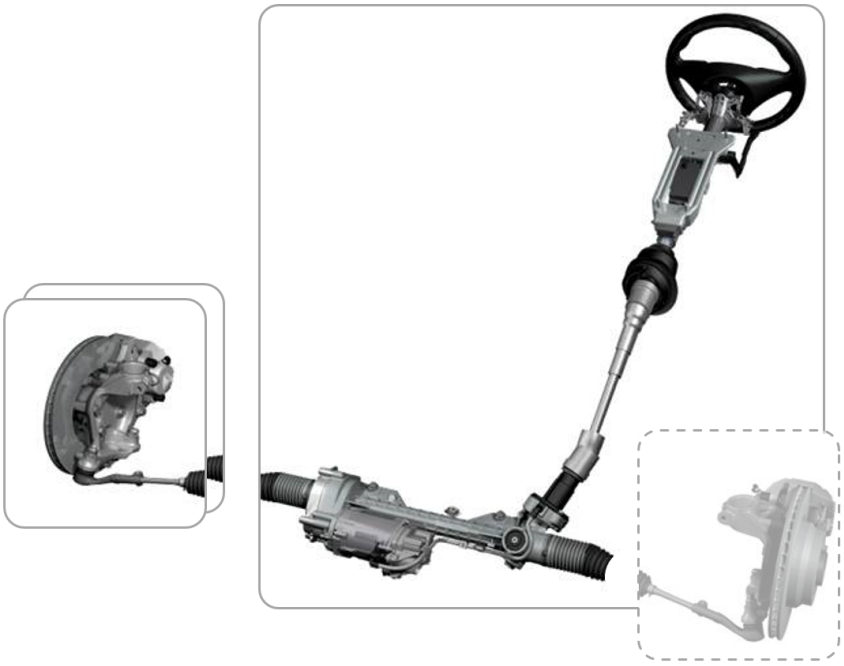

Figure 1: Coupled system consisting of front axle and steering subsystems

by the effective rod forces, the two connection points of the steering rack to the left and right tie rod may be reduced to a single-degree-of-freedom interface between the subsystems. In other words, the suspension subsystem is made up of the two axle halves, acting with their effective rod forces upon the steering rack. From Fig. 4, introduced later in the text and showing a multibody model of the front axle, it can be clearly understood that the entire front axle can be considered as one four-pole subsystem since only the resulting force on the steering rack, assumed to be rigid, is relevant. As the masses and dynamic stiffnesses of ball joint and tie rod have low impact on the global system dynamics in the frequency range up to 30 Hz and as they are arranged symmetrically to the steering rack, this simplification is acceptable.

2.2. Mechanical Four-Poles Applied to Steering Design

An abstract representation of two interconnected subsystems using mechanical four-poles according to [7, 12, 13] is shown in Fig. 2. When the predefined excitation force F_1 acts on the input port of the front axle subsystem, the wheel responds with the associated (longitudinal) velocity v_1. At the output port of the steering subsystem, the reaction force F_3 and / or the velocity response v_3 arise. These variables represent the torque and the angular velocity of the steering wheel, which can be measured on the testrig by means of a torque sensor and radially displaced accelerometers. For the sake of consistency, they are scaled to the translational degree of freedom of the rack using the transmission ratio from the rack and pinion drive. The rack force F_2 and the related velocity v_2 constitute the interface variables between the front axle and the steering. Already known as translational degrees of freedom from the real system, they do not need to be transformed any further. In practice, they can be measured by tie rod integrated strain gauges and accelerometers placed upon the rack.

For the global transfer matrix $\mathbf{A}_G$ of the coupled (vehicle) system formed by a serial connection of the two subsystems $\mathbf{A}_1$ and $\mathbf{A}_2$, one finds:

$$\begin{bmatrix} F_1 \\ v_1 \end{bmatrix} = \mathbf{A_1 A_2} \begin{bmatrix} F_3 \\ v_3 \end{bmatrix} = \mathbf{A_G} \begin{bmatrix} F_3 \\ v_3 \end{bmatrix}, \text{ with } \mathbf{A_G = A_1 A_2}. \tag{1}$$

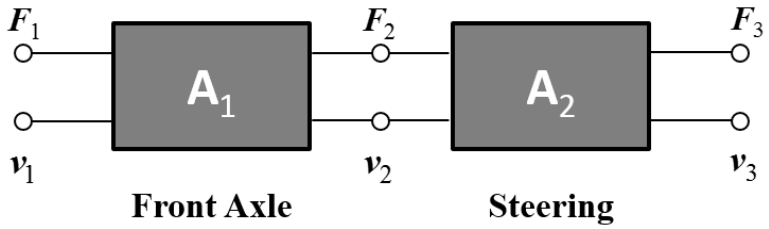

Figure 2: Four-pole model of the coupled front axle and steering subsystems

The dynamics of the coupled system can be expressed by means of the complex frequency response functions A_G^{ij} and the four input and output ports as following:

$$F_1 = A_G^{11} F_3 + A_G^{12} v_3, \tag{2}$$
$$v_1 = A_G^{21} F_3 + A_G^{22} v_3. \tag{3}$$

The interface force and velocity at the steering rack can be calculated from the steering transfer matrix and the outputs of the coupled system:

$$F_2 = A_2^{11} F_3 + A_2^{12} v_3, \tag{4}$$
$$v_2 = A_2^{21} F_3 + A_2^{22} v_3. \tag{5}$$

Useful steering feedback is defined as the ratio between the reaction force F_3 at the rim of the clamped ($v_3 \approx 0$) steering wheel to the excitation force F_1 at the rolling wheel. According to Eq. 2, this is equivalent to the inverse of A_G^{11}:

$$\left.\frac{F_3}{F_1}\right|_{v_3=0} = (A_G^{11})^{-1}. \tag{6}$$

Undesired (i. e. disturbing) feedback is defined as the resulting acceleration or velocity v_3 at the freely oscillating steering wheel ($F_3 = 0$) caused by the excitation force F_1 at the wheel. Using again Eq. 2, this is expressed by the inverse of A_G^{12}:

$$\left.\frac{v_3}{F_1}\right|_{F_3=0} = (A_G^{12})^{-1}. \tag{7}$$

Both frequency response functions of the coupled system A_G^{11} and A_G^{12}, which represent steering characteristics at vehicle level, result in turn from two frequency response functions of each of the two subsystems connected in series, as introduced in Eq. 1:

$$\mathbf{A_G = A_1 A_2} \Rightarrow A_G^{11} = A_1^{11} A_2^{11} + A_1^{12} A_2^{21}, \tag{8}$$
$$\mathbf{A_G = A_1 A_2} \Rightarrow A_G^{12} = A_1^{11} A_2^{12} + A_1^{12} A_2^{22}. \tag{9}$$

If one of these two global transfer coefficients are considered to impose a requirement to the vehicle design, two frequency response functions for both of the subsystems have to be either identified (if their design is available already) or specified in terms of permissible vibration levels. The relevant dynamic properties A_1^{ij} of the front axle subsystem can be determined independently from the characteristics of the steering subsystem A_2^{ij}.

The meaning of some of the transfer coefficients needed in Eq. 8 and Eq. 9 will now be shortly discussed. At fixed rack, the force transmission ratio of the axle corresponds to

$$A_1^{11} = \left.\frac{F_1}{F_2}\right|_{v_2=0}. \tag{10}$$

This quantity describes the frequency dependent ratio of the excitation force F_1 at the wheel to the reaction force F_2 at the fixed rack ($v_2 = 0$). Similarly, at freely oscillating rack the so-called transfer impedance of the axle is defined as

$$A_1^{12} = \left.\frac{F_1}{v_2}\right|_{F_2=0}. \tag{11}$$

Here, the transfer impedance represents the frequency response function from excitation force F_1 at the wheel to the velocity response v_2 at the non-fixed rack ($F_2 = 0$).

Regarding the relevant dynamic properties A_2^{ij} of the steering, there are different frequency response functions noted in Eq. 8 and Eq. 9. Which of these are actually needed depends on whether the vehicle characteristic A_G^{11} or A_G^{12} is of interest. If we focus on disturbing steering feedback represented by the vehicle frequency response function A_G^{12}, the following frequency response functions of the steering must be specified according to Eq. 9: Firstly, the transfer impedance from the excitation force at the rack to the velocity response at the freely oscillating steering wheel

$$A_2^{12} = \left.\frac{F_2}{v_3}\right|_{F_3=0}, \tag{12}$$

and secondly, the velocity transmission ratio for the freely oscillating steering wheel, which is

$$A_2^{22} = \left.\frac{v_2}{v_3}\right|_{F_3=0}. \tag{13}$$

2.3. Setting Subsystem Targets Derived from the System Requirements

Eq. 9 allows to derive subsystem targets A_1^{ij} and A_2^{ij} with reference to global system requirements such as the desired vehicle impedance A_G^{12}. One may derive a limiting curve to each subsystem frequency response function if all the other frequency response functions are determined.

Beforehand, the vehicle target regarding steering vibration must be transformed into a compatible form. Undesired steering vibration is typically assessed at vehicle level by tolerable steering wheel acceleration amplitudes a_3 over vehicle speed v_x related to a certain imbalance mass m_{imb} applied to one of the front wheels. With the radial distance r of the imbalance mass m_{imb} to the center of the rolling wheel with radius r_{whl}, the excitation force amplitude can be written as

$$F_1(m_{imb}, \omega) = m_{imb} r (v_x / r_{whl})^2 = m_{imb} r \omega^2. \tag{14}$$

To eliminate any human influence, the driver keeps his hands off the steering wheel during measurement. Physically, this corresponds to the boundary condition $F_3 = 0$. Using complex four-pole coefficients, as noted in Eq. 2, the vehicle target property can be related to the inverse of A_G^{12} which is called mechanical inertance:

$$G(j\omega) = \left.\frac{a_3(m_{imb}, \omega)}{F_1(m_{imb}, \omega)}\right|_{F_3=0} = j\omega \left.\frac{v_3(m_{imb}, \omega)}{F_1(m_{imb}, \omega)}\right|_{F_3=0} = j\omega (A_G^{12})^{-1}. \tag{15}$$

The vehicle target value in terms of maximum admissible steering wheel acceleration amplitude $a_{3,max}(m_{imb}, \omega)$ for a given imbalance mass and frequency can also be expressed as permissible mechanical intertance

$$G_{max}(\omega) = \left.\frac{a_{3,max}(m_{imb}, \omega)}{F_1(m_{imb}, \omega)}\right|_{F_3=0}, \tag{16}$$

where the exciting force $F_1(m_{imb}, \omega)$ is already given by Eq. 14. The vehicle target is met if the magnitude of the actual mechanical inertance $G(j\omega)$ is lower than required limit values $G_{max}(\omega)$ over vehicle speed

$$G(j\omega) \leq G_{max}(\omega). \tag{17}$$

In other words, the magnitude of the global transfer impedance of the coupled system needs to exceed a lower treshold, which is

$$\left|A_G^{12}\right| = \left|A_1^{11}A_2^{12} + A_1^{12}A_2^{22}\right| \geq \frac{\omega}{|G_{max}(\omega)|}. \tag{18}$$

Inequality Eq. 18 must be satisfied for all frequencies ω and may be solved to any of the four-pole coefficients involved. This yields requirements in terms of limiting values to the dynamics of the subsystem the respective coefficient belongs to. By this means, the subsystems can be assessed separately from each other as will be discussed next.

2.3.1. Derivation of Necessary and Sufficient Limits to the Four-Pole Coefficients

Solving Eq. 18 in order to derive requirements to four-pole coefficients such as A_2^{12} or A_2^{22} of the steering is complicated by the fact that the magnitude of the sum of complex coefficients differs from their summed magnitudes. Fig. 3 illustrates this property using the example of complex numbers $z_{1,2}$. Using triangle inequalities, the true absolute value of the summed up complex numbers can be bounded by two extreme values, which are the sum and the difference of their absolute values. In the same manner, the exact solution of Eq. 18 can be estimated by an upper and lower limit

$$\left|A_1^{11}A_2^{12}\right| + \left|A_1^{12}A_2^{22}\right| \geq \left|A_G^{12}\right| \geq \left|\left|A_1^{11}A_2^{12}\right| - \left|A_1^{12}A_2^{22}\right|\right|. \tag{19}$$

Now, Eq. 18 may be solved for any of the four-pole coefficients which are found on the right and left side of the expression. For instance in case of the steering transfer impedance A_2^{12}, the following inequalities arise

$$\left|A_{2,\,necess}^{12}\right| \geq \left(\frac{\omega}{|G_{max}(\omega)|} - \left|A_1^{12}A_2^{22}\right|\right)\frac{1}{|A_1^{11}|}, \tag{20}$$

$$\left|A_{2,\,suff}^{12}\right| \geq \left(\frac{\omega}{|G_{max}(\omega)|} + \left|A_1^{12}A_2^{22}\right|\right)\frac{1}{|A_1^{11}|}. \tag{21}$$

Eq. 20 refers to the maximum of the combined magnitude which is the upper limit to the vehicle performance in terms of A_G^{12} and correspondingly the maximum expectable steering transfer impedance A_2^{12}. If this necessary constraint is not satisfied for at least one single frequency ω, at least partial non-compliance of the desired behavior of the vehicle must be expected.

Likewise, Eq. 21 refers to the minimum of the combined magnitude which is the lower limit both to the vehicle performance and the steering transfer impedance. If this sufficient constraint is satisfied for all frequencies, full compliance with the limiting curve at vehicle level is assured.

2.3.2. Derivation of Exact Limits to the Four-Pole Coefficients Depending on Phase-Angles

Even though the requirements derived by Eq. 20 and 21 are rather estimates than accurate limits, the preliminary evaluation of each subsystem from experimental or virtual tests is feasible now. No more investigation is needed if the necessary constraint is violated (target will be definitely missed) or the sufficient contraint is fulfilled (target will be definitely met). But if the respective four-pole coefficient lies in between those boundaries, a more accurate calculation of the limits is recommendable. Exact limits are useful to avoid unjustified rejection of subsystem designs as well as excessive requirements, which unnecessarily increase manufacturing effort.

As demonstrated by Fig. 3, the exact combined magnitude of the complex numbers z_1 and z_2 can be calculated, provided that not only their magnitudes but also their phase angles are known. For this purpose, the four-pole coefficients of Eq. 18 are rewritten in the polar form

$$\left|\left|A_1^{11}\right|\left|A_2^{12}\right|\exp(j(\varphi_1+\varphi_2)) + \left|A_1^{12}\right|\left|A_2^{22}\right|\exp(j(\varphi_3+\varphi_4))\right| \geq \frac{\omega}{|G_{max}(\omega)|}, \tag{22}$$

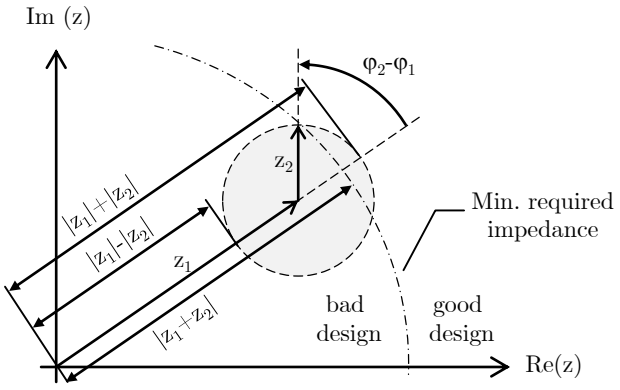

Figure 3: Argand Diagram of composed complex numbers and their bound values

where $\varphi_{1,2,3,4}$ denote the phase angle of the respective four-pole coefficient. With reference to Fig. 3, the two parts of Eq. 22 represent the complex numbers

$$z_1 = \left|A_1^{11}\right| \left|A_2^{12}\right| \exp(j(\varphi_1 + \varphi_2)), \tag{23}$$

$$z_2 = \left|A_1^{12}\right| \left|A_2^{22}\right| \exp(j(\varphi_3 + \varphi_4)). \tag{24}$$

Taking into account that the left side of Eq. 22 represents the magnitude of the geometrically superimposed complex numbers, Eq. 22 can be rewritten as

$$\sqrt{\left(\left|A_1^{11}\right|\left|A_2^{12}\right|\right)^2 + \left(\left|A_1^{12}\right|\left|A_2^{22}\right|\right)^2 + 2\left|A_1^{11}\right|\left|A_2^{12}\right|\left|A_1^{12}\right|\left|A_2^{22}\right| \cos\left((\varphi_1 + \varphi_2) - (\varphi_3 + \varphi_4)\right)} \geq \frac{\omega}{|G_{max}(\omega)|}. \tag{25}$$

By solving Eq. 25 to any four-pole coefficient to be specified, both magnitude and phase of the chosen coefficient can be separated from all other coefficients. In case of the steering impedance, for instance, this yields Eq. 26 characterizing the magnitude $\left|A_2^{12}\right|$ as function of the phase angles

$$\left|A_2^{12}\right|^2 + 2\left|A_2^{12}\right| \frac{\left|A_1^{12}\right|\left|A_2^{22}\right|}{\left|A_1^{11}\right|} \cos(\phi) + \left(\frac{\left|A_1^{12}\right|\left|A_2^{22}\right|}{\left|A_1^{11}\right|}\right)^2 \geq \left(\frac{\omega}{|G_{max}(\omega)|\left|A_1^{11}\right|}\right)^2, \tag{26}$$

where $\phi = \varphi_1 + \varphi_2 - \varphi_3 - \varphi_4$ denotes the combined phase angle after superimposition of all complex four-pole coefficients. The roots of the quadratic equation Eq. 26 represent exact lower limit values to the amplitude of the steering impedance

$$\left|A_2^{12}\right|_{1,2} \geq \frac{1}{A_1^{11}} \left(-\left|A_1^{12}\right|\left|A_2^{22}\right| \cos(\phi) \pm \sqrt{\left(\frac{\omega}{|G_{max}(\omega)|}\right)^2 + \left(\cos^2(\phi) - 1\right)\left(\left|A_1^{12}\right|\left|A_2^{22}\right|\right)^2} \right), \tag{27}$$

where only positive values are meaningful. It is obvious that for $\phi = 0$ and $\phi = \Pi$ Eq. 27 simplifies to the necessary and sufficient constraints as defined by Eq. 20 and 21.

Similar to Eq. 27, which is derived exemplarily for the steering impedance, exact limits may be derived to each of the four-pole coefficients in the same manner. Let us note that Eq. 20, 21 and 27 allow for setting targets on a selected transfer coefficient of subsystem $\mathbf{A}_2$, but that the right hand side also contains another coefficient of subsystem $\mathbf{A}_2$. This is however not a problem in the design process since, as will be shown later, specific design parameters affect only one of those coefficients.

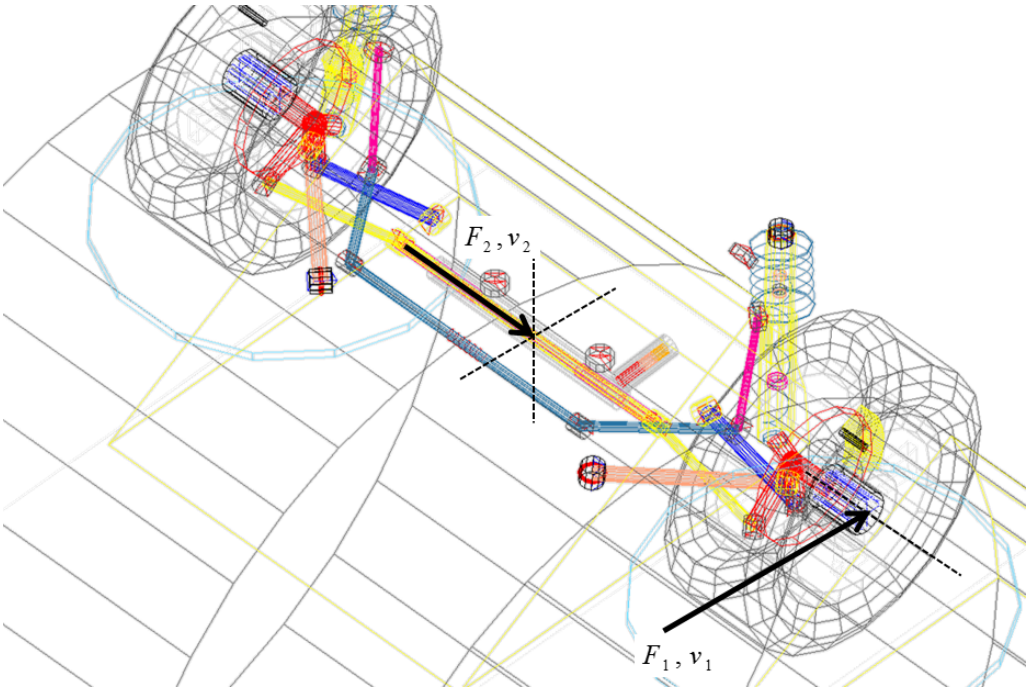

Figure 4: MBS model of the front axle without steering on virtual roller-testrig under imbalance excitation [16]

3. Vehicle Targets and Subsystem Identification

Applying the methodology developed above, it is feasable to derive requirements to either the steering or the front axle if following prerequisites are satisfied: Firstly, given vehicle targets must be reformulated in terms of required impedance of the coupled system. Secondly, actual or estimated dynamics of one of the subsystems must be determined by simulation or experiment. Then, corresponding limiting curves to the unknown subsystem may be derived. In this paper, the system of interest is a passenger car with the subsystems electric power-assisted steering and McPherson front suspension. This subsystem combination represents a conceptual layout which is often found in both small and medium cars.

3.1. Defining Vehicle Targets

As mentioned above, vehicle targets regarding disturbing steering vibration are expressed in form of permissible amplitudes of steering wheel acceleration over vehicle speed as indicated by the red area in the upper graph of Fig. 11 in Section 4.3 of this paper. With reference to industrial standards [14, 15], the graph is divided into sections with constant amplitude rise and an intermediate section with constant amplitude values over frequency, which is typical for sensitivity of the human body exposed to vibration. As stated by Eq. 16, the permissible amplitudes of the tangential acceleration at the steering wheel $a_{3.max}$ refer to a predefined excitation force F_1 caused by a certain imbalance mass applied at one of the front wheels. The required magnitude of the transfer impedance of the vehicle A_G^{12} is obtained by inserting Eq. 14 and Eq. 16 into Eq. 18. This dynamic property of the global system is shown in the lower graph of Fig. 11 on page 15. Note that, due to the inversion of the vehicle target in terms of permissibe acceleration (Eq. 18), the transfer impedance respresents a lower limiting curve, which must be exceeded for all frequencies. The colored section below the limiting curve illustrates this restriction. Vehicle targets will be met if the actual impedance lies completely outside the colored area.

3.2. Identification of the Front Axle Dynamics

Besides vehicle targets, Eq. 18 contains dynamic properties A_1^{ij} of the front axle, which have to be determined before requirements to the steering characteristics can be derived. The transfer impedance and

the force transmission ratio of existing or proposed front axle designs may be identified by means of multi-body simulation performing two virtual experiments in the time domain, defined by Eqs. 10 and 11. As for this purpose the steering rack has to be fixed rigidly or disconnected from the steering gear (no motion/ no forces), the front axle dynamics is analyzed isolated from any steering characteristics except for the steering linkage.

Fig. 4 on the previous page shows the simulation model of the McPherson front axle mounted on a purpose-built but still universal applicable virtual roller-testrig, as developed in [16]. To analyze the dynamic properties of this subsystem, the testrig features virtual actuators who allow to apply arbitrary excitation forces to the hubs or wheels. Virtual sensors measure the resulting forces and/or motions at the interface to the steering rack. In case of imbalance excitation, the point mass fixed to the rim produces an excitation force rotating together with the wheel. Although the imbalance excitation when regarding steering vibration is applied only to one wheel of the axle, the chosen mass corresponds to typical imperfections on both wheels which are in antiphase to each other in the worst case.

The rollers are speed controlled starting from standstill with increasing velocity over time, in order to cover all frequencies occuring during realistic manoeveurs of the vehicle during steady-state driving. In case of circular imbalance mass forces, the excitation frequency corresponds to the wheels angular velocity which is proportional to the vehicle driving speed, see Eq. 14. The Fourier transform of the data generated in the time domain, represents the subsystem dynamics linearized along the actual operating curve, which depends on the manoeuver, the suspension setup and the excitation mechanism.

3.3. Identification of the Steering Dynamics

Besides vehicle targets and front-axle characteristics also the dynamic properties A_2^{ij} of the steering are essential to solve Eq. 18 for subsystem requirements. They can be derived either by virtual or by experimental analysis, depending on the degree of maturity of the steering subsystem and its components. During the phase of conceptual layout, only simulation models of the steering are available to calculate its dynamic properties on a virtual testrig. Physical models which prove suitable for this purpose are introduced by [17] and [18]. These models cover both mechanical and electrical components of the steering subsystem extending from the rack to the steering wheel.

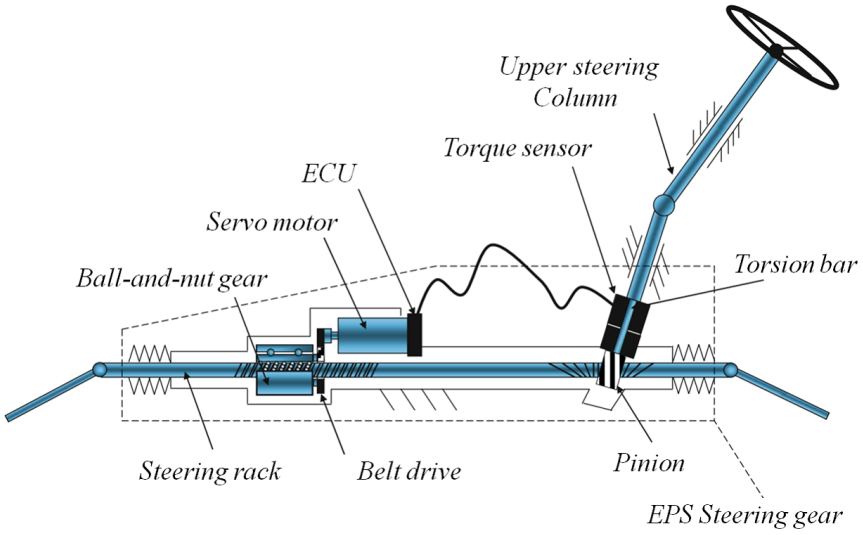

Figure 5: Basic Principle of Electric Power Steering with parallel-axis drive according to [19]

Fig. 5 illustrates the basic principle of electric power steering (EPS) with parallel-axis drive.The driver's manual torque applied to the steering wheel is fed to the steering pinion via the upper steering column. At the steering rack, the pinion torque is assisted by the torque of the electric servo motor which is amplified

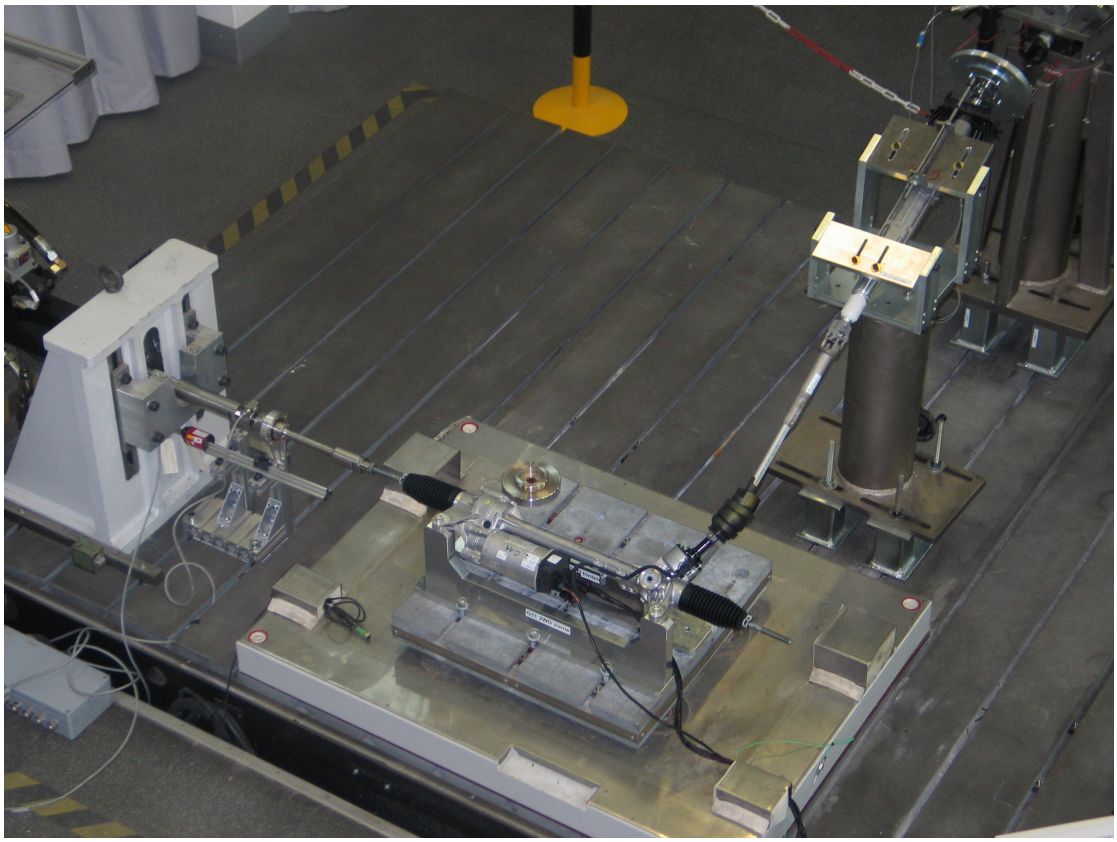

Figure 6: Experimental subsystem testrig to identify the dynamics of a steering prototype

by a belt drive and a ball-and-nut gear. The commanded assisting torque depends on the driver's torque, measured at the torsion bar, and on the vehicle states such as driving speed, lateral acceleration and yaw rate. As the steering pinion and the ball-and-nut gear are both connected to the rigid steering rack, their angular velocities are coupled strongly. For this reason, it is the motor torque which is controlled while the motor speed follows the translational velocity of the steering rack according to the driver's angle input at the steering wheel. The summed translational force is propagated to the left and right wheels via two tie rods which are part of the front suspension. As only effective forces between the steering and the suspension are of interest, the two linkages can be treated as single coupling interface of the two subsystems as explained earlier in Section 2.1.

Once first prototypes of the steering are accessible, their dynamics is evaluated on experimental testrigs, like the one shown in Fig. 6. For this purpose, the upper steering column connected to the steering gear is aligned identically to the mounting position in the vehicle. The steering wheel is replaced by a simple disc featuring the same inertia, which can be actuated, left free or clamped fixed to the testrig. Torque and angular acceleration are measured by external sensors applied to the disc. At one end of the steering rack, harmonic excitation forces are applied by a hydraulic jack with force control. Effective force and translational acceleration are again measured by external sensors applied to the rack. In addition to these essential interface measurements, internal measurements of the servo drive are recorded during operation on the testrig, such as sensed pinion torque, motor torque and speed. Please note that the internal measurements are not necessary to determine the four-pole coefficients of the steering, but they are useful to check proper function of the servo drive on the testrig compared to real driving.

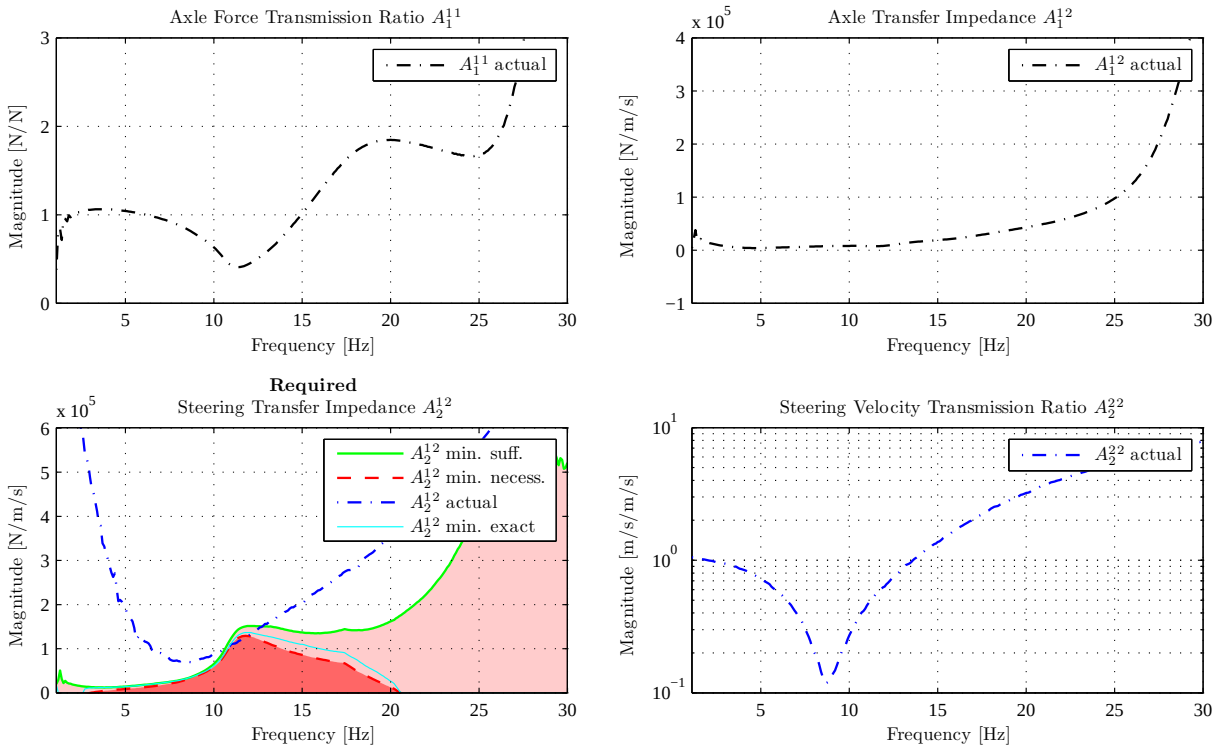

Figure 7: Limiting curves to required steering dynamics computed for a given front axle dynamics

4. Derivation of Requirements to Subsystems

Requirements to the subsystems are derived in this section using the theory introduced in Section 2. Linear behavior of the subsystems is assumed. Two use-cases are covered, which are typical for aligned development processes at automotive applications. Firstly, requirements to the steering subsystem are derived based on vehicle targets and assumed front-axle dynamics. Secondly, requirements to the front axle subsystem are derived in analogous manner, based on vehicle targets and assumed steering dynamics.

4.1. Deriving Limits to the Steering Dynamics

Usually, steering systems are tested virtually or experimentally by applying external forces to the steering wheel and measuring reactional forces or motions at the rack or vice versa. Based on virtual designs of the front axle, suitable amplitudes regarding rack travel and rack force as well as basic steering design parameters such as the rack-and-pinion gear ratio are defined at this stage of development. The following subsections demonstrate how requirements at subsystem level may be derived in order to assess subsystem testing results.

4.1.1. Necessary and Sufficient Limits to the Steering Impedance

Regarding disturbing steering vibration, the above mentioned transfer impedance A_2^{12} and velocity transmission ratio A_2^{22} are the two relevant properties to be assessed when it comes to virtual or experimental testing of a steering prototype (see Section 2.2). In case of the transfer impedance amplitude, suitable limiting curves can be derived by means of Eqs. 20 and 21 if the nominal dynamics of the front axle A_1^{ij} and the velocity transmission ratio of the steering, which is mainly affected by the design of the upper steering column, are known. The chart on the bottom left of Fig. 7 shows both necessary (red dashed) and sufficient (green solid) limiting curves to the minimal required steering transfer impedance based on virtually obtained front axle and steering subsystem properties. These two types of requirements can be calculated without knowing actual phase angles as only the magnitudes of the four-pole coefficients are needed. However, if

the phase angles of all the four-pole coefficients are known additionally, it is feasible to calculate the actual exact limiting curve (cyan solid) which runs between the necessary and the sufficient limits.

All of these limiting curves to the minimal required steering transfer impedance rely on front axle dynamics known from multi-body simulation (see the two charts on the top of Fig. 7) and the calculated velocity transmission ratio (chart on the bottom right of Fig. 7), which in turn is also a property of the steering subsystem. Thus it appears, that the two four-pole coefficients of the steering interact with each other, i. e. varying velocity transmission ratio A_2^{22} involve changes of the required transfer impedance A_2^{12}, for a given vehicle target A_G^{12}. However, the transmission ratio is assumed to be affected only by design changes within the upper steering column (such as column stiffness and steering wheel inertia) and not by usual design changes of the steering gear and the servo drive. Considering the low frequency range here, where the rack and pinion gear behaves almost rigidly, this assumption is acceptable. As a showcase, also the actual transfer impedance of a steering system being under design is shown additionally (blue dash-dotted line) in the bottom left of Fig. 7. If the actual curve runs completely outside the colored area, the steering design in combination with the assumed front axle will meet the vehicle targets introduced in Section 3.1. But if the red colored area is entered even partially, vehicle targets will be missed. If the curve enters the rose colored but not the red colored area, one has to take phase angles into account.

4.1.2. Phase-Angle Dependent Limits to the Steering Impedance

According to Eq. 27, the relevant combined phase angle ϕ results from the superimposition of all the four-pole coefficients. This implies that the (exact) magnitude of tolerable steering transfer impedance finally depends on its own phase angle. If the phase angle of the steering is measured during the experimental test, the emerging magnitude can thus be assessed with reference to the exact limiting curve. But if the phase angle of the interesting four-pole coefficient is still unknown, which is the case if requirements have to be derived without having access to actual measurements or simulation results, it is useful to calculate limiting curves (iso-lines) for a set of constant values of either one of the individual phase angles $\varphi_{1,2,3,4}$ or the combined phase angle ϕ. The latter is used in this example, as the combined phase angle demonstrates the relationship between suffcient, necessary and phase-dependent limiting curves in a comprehensible manner.

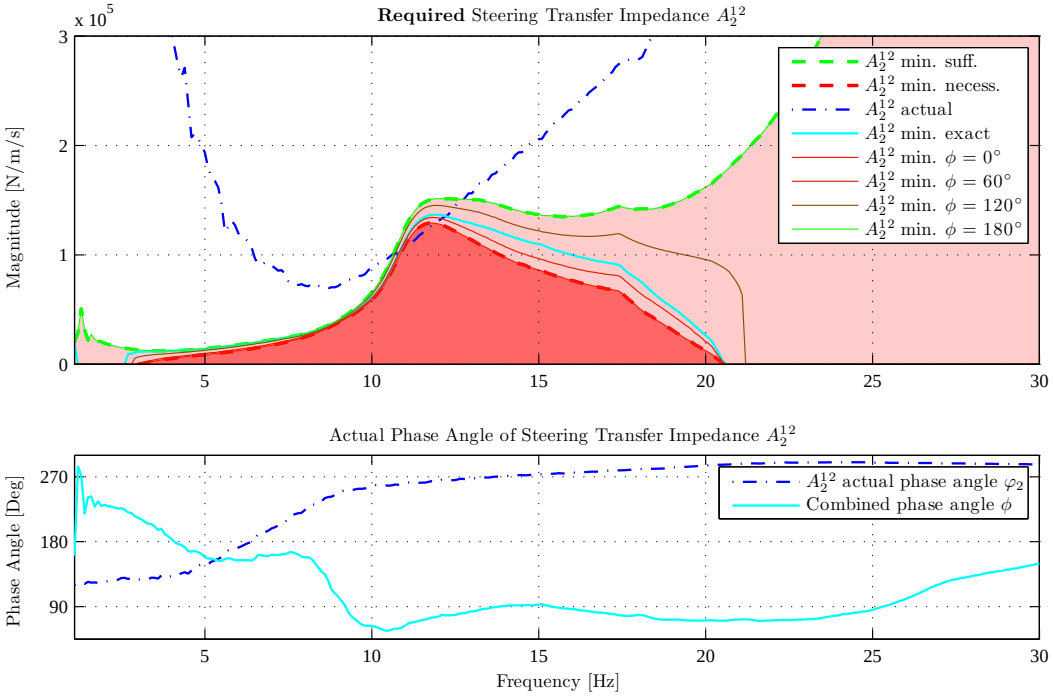

Figure 8: Limiting curves to required steering impedance depending on phase angles

The top chart of Fig. 8 indicates such iso-lines, for constant phase angles exemplarily, representing exact limiting curves to the steering transfer impedance amplitude. As shown in the bottom chart of Fig. 8, the individual phase angle of the steering transfer impedance (blue dash-dotted), known from the measurements, and the combined phase angle of all the four-pole coefficients (cyan solid), derived from calculation, differ reasonably from each other. The combined phase angle proves advantageous to check the plausibility of the course of the exact limiting curve (cyan solid) shown in the top chart of Fig. 8: A combined phase angle $\phi = 0°$ results in a limiting curve congruent to the necessary limit, whereas the sufficient limit is reached for $\phi = 180°$. Note that the exact limiting curves can be derived with reference to the actual phase angle of the steering transfer impedance as well if it is feasible to measure it. Thus the magnitude of the steering transfer impedance can be assessed immediately during the measurement procedure which still can take place at the supplier.

4.1.3. Robust Limits to the Steering Impedance Coping with Uncertainties

Typically, the steering subsystem has to cope with uncertain parameter values, e. g. of the steering wheel inertia, depending on the customers choice of options. The right chart of Fig. 9 illustrates varying dynamics of the upper steering column, i. e. the velocity transmission ratio A_2^{22}, caused by steering wheel inertiae scattering up to +/- 20 % around the nominal value. As a result, there is no unique solution for the limiting curves to be used as requirement to the steering transfer impedance A_2^{12} covering all possible velocity transmission ratios. In fact, the necessary (red dashed) and sufficient (green solid) limiting curves spread to "limiting zones" which are filled gray in the left chart of Fig. 9. Likewise the actual steering transfer impedances themselves shows considerable deviations from the nominal curve (blue dashed). Obviously, the steering wheel inertia influences both design-relevant four-pole coefficients of the steering at the same time.

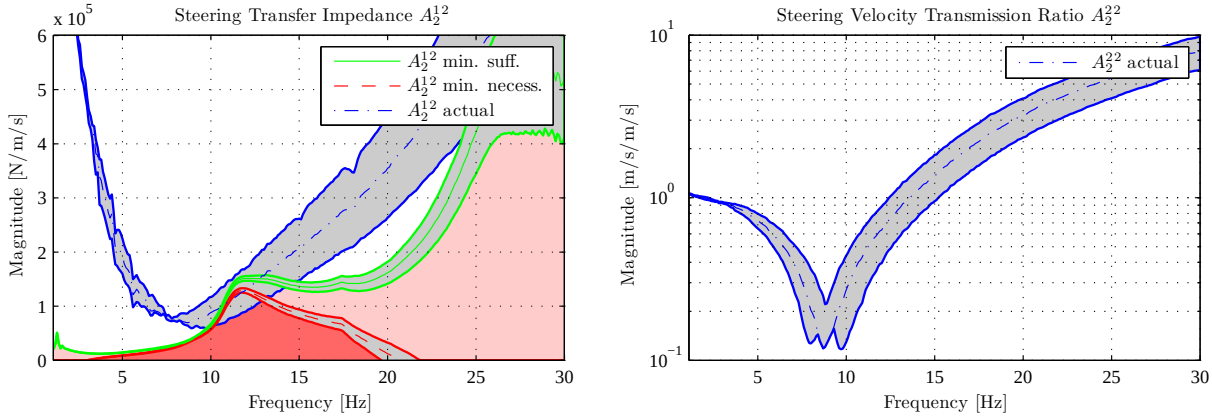

Figure 9: Robust Limiting Zones to required steering impedance due to varying steering wheel inertiae

Yet, vehicle targets are fulfillable despite all of these variances if the spread of the steering transfer impedance curves lies outside (i. e. above) the necessary limiting zone (red-gray). Moreover, target fulfillment is guaranteed for all frequencies and values of steering wheel inertiae if all impedance curves run outside the sufficient limiting zone (green-gray). Alternatively, presuming the phase angles of all other four-pole coefficients are known from virtual or experimental measurements, the exact limiting zone can be calculated for chosen phase angles or the actual phase angle. Such phase-dependent limiting zones, not shown in Fig. 9 for clarity, represent exact requirements which are relaxed compared to the sufficient limits.

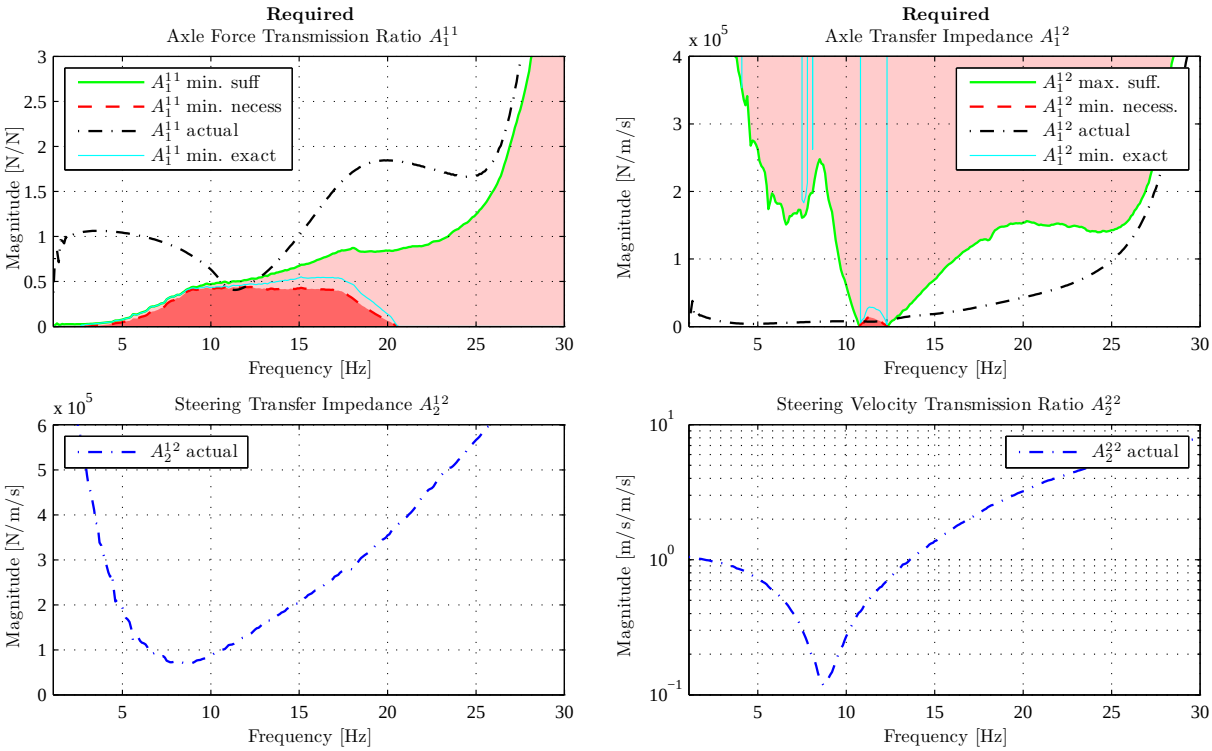

Figure 10: Limiting curves to required front axle dynamics computed for a given steering dynamics

4.2. Deriving Limits to the Front Axle Dynamics

If the steering subsystem exists already, the introduced methodology can also be used to assess conceptual front axle layouts during the whole design process of the vehicle. As most vehicle models are designed as derivatives of a whole vehicle "family", they often share the steering subsystem with only few design modifications. In this case the question is, whether conceptual designs of the front axle are compatible with existing steering subsystem in terms of fulfillment of vehicle targets.

Similar to Section 4.1, where limits to the steering are derived, again Eq. 20, Eq. 21 and Eq. 27 are useful to derive limits to the front axle subsystem by solving these equations for the involved coefficients of the front axle subsystem. Limiting curves to the force ratio A_1^{11} can be derived depending on the transfer impedance A_1^{12} and the coefficients of the steering. Vice versa, limiting curves to the transfer impedance A_1^{12} can be calculated as a function of the force ratio A_1^{11} and the steering dynamics.

In contrast to the steering, the front axle usually shows big variance both regarding the force ratio and the transfer impedance when modifying the conceptual layout. I. e. the design relevant front axle dynamics are strongly interdependent and must be "monitored" simultaneously. For this reason, Fig. 10 features areas of good and bad performance for both the front axle force ratio and the front axle transfer impedance. Again, sufficient (green), necessary (red) and exact (cyan) limiting curves are plotted in comparison to actual dynamics of the current layout (black dashed-dotted). To compute the exact limiting curves, measured phase angles of the steering are combined with calculated phase angles of the front axle.

Please note, that the requirements to the force ratio A_1^{11} represent lower limiting curves while at the transfer impedance A_1^{12} the sufficient requirement constitutes an upper limiting curve and the necessary requirement states a lower limiting curve. This can be explained by Eq. 19 where the relevant four-pole coefficients are located on opposite sides of the sum or difference respectively. For more details on the graphical interpretation of the limiting curves the reader is recommended to AppendixA.

According to Fig. 10, the current axle design does not comply with vehicle targets, as the area of bad performance (red) is penetrated in the frequency range of about 11 Hz. A valid front axle design cannot be

claimed before both front axle dynamics run completely outside their red areas, which could be achieved for instance by increasing the damping within the indicated frequency range.

4.3. Prediction of Vehicle Performance after Assembling

Eq. 18 enables the prediction of actual transfer impedance of the assembled vehicle system A_G^{12} based on virtually or experimentally determined four-pole coefficients of the front axle and steering subsystems. Moreover, the vibration amplitude level at the vehicle steering wheel a_3 can be calculated using Eq. 15. The therefore required exciting wheel force $F_1(m_{imb}, \omega)$, as given by Eq. 14, is predefined by the specific imbalance mass m_{imb} the vehicle target values correspond to. The excitation frequency ω is porportional to vehicle speed, assuming only first order excitations are relevant and higher harmonics might be neglected. As will be illustrated next, both actually measured and theoretically permissible four-pole coefficients may be used for prediction of vehicle performance, in order to demonstrate how potential target deviations may be solved by modified subsystem dynamics of steering or front axle.

4.3.1. Target Achievement by Modified Steering Dynamics

Fig. 11 shows predicted global system dynamics assembled from actually measured four-pole coefficients (black solid) of front axle and steering. The upper diagram contains the steering wheel acceleration[1] to be expected, whereas the lower graph indicates the vehicle transfer impedanceA_G^{12}, introduced as vehicle target in Section 3.1. Obviously, the combined front axle and steering designs do not fully comply with vehicle targets. Especially in the frequency range around 11 Hz, the curves penetrate the forbidden area, which indicates steering vibration to be higher than allowed. Remember that this result is consistent with target deviations on subsystem level, which were already observed in Sections 4.1 and 4.2.

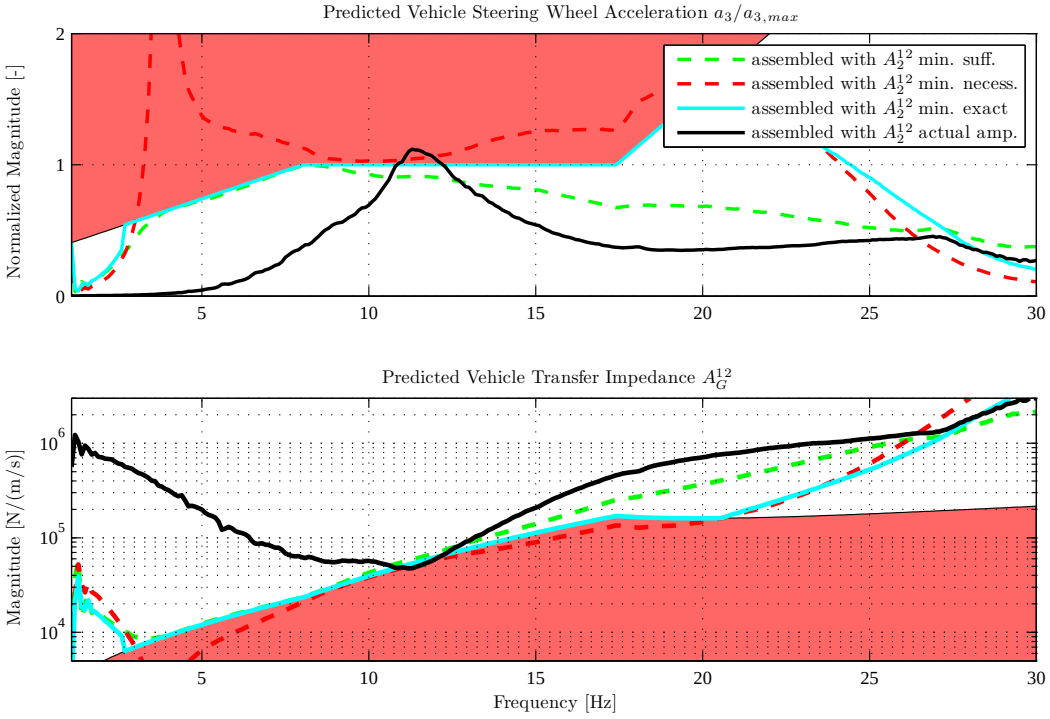

Figure 11: Vehicle Performance based on different Steering Dynamics compared to Vehicle Targets according to VDI2057 [14]

[1] the steering wheel acceleration is normalized with tolerable values $a_{3,max}$ at vehicle speed of 80 kmph

Additionally, expected vehicle performances based on *limiting curves* instead of *actual dynamics* of the steering subsystem are plotted in Fig. 11. The prediction is done by insertion of permissible steering four-pole coefficients into Eq. 18, for instance limiting curves to the steering transfer impedance A_2^{12}.

The predicted curve based on the *exact limit* (cyan) to A_2^{12}, which is a subsystem requirement considering actual phase angles, results exactly in the permissible steering vibration amplitudes for all frequencies. The *sufficient limiting curve* (green dashed) leads to target achievement as well, exploiting permissible values in a widespread area of frequencies. But the *necessary limiting curve* (red dashed) does not proof very valuable, as the therefrom resulting vibration level overshoots massively the permissible values.

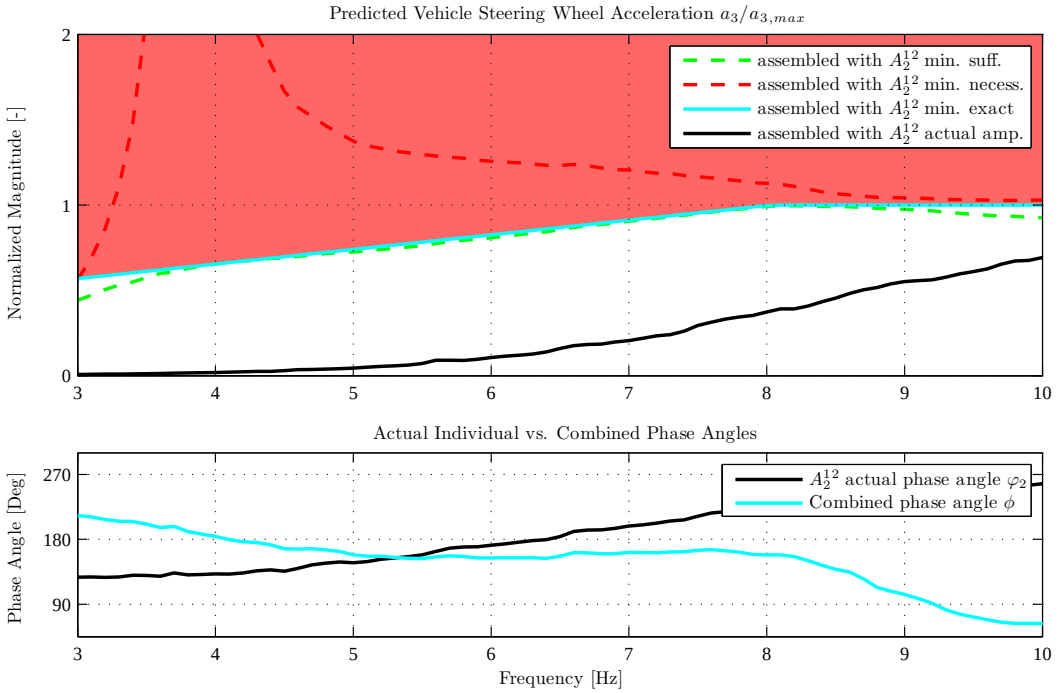

Figure 12: Comparison of Phase Angle and Predicted Vehicle Performance using different limiting curves

The failure of this limiting curve may be explained by taking a look at the combined phase angle ϕ, shown in the lower graph of Fig. 12: Due to the fact that the actual combined phase angle is close to 180° (anti-phase), per definition the necessary limiting curve is not very trustable. Remember that the necessary limit is only a good estimate of the exact limit if the phase angle is close to 0° (in-phase), which can be explained by the schematic argand diagram shown in Fig. 3. At the same time, the combined phase angle is the explanation for the good results arising from assembling with the sufficient limiting curve. These results are close to those derived with the exact limit, which represents theoretically the maximum permissible values. But even the exact limit leads to maximum permissible vibration amplitudes only within the frequency range, where exact limits are calculable. According to Fig 7, this is the case from about 2 to 21 Hz. Below and above there exist no exact limits, i. e. the permissible values can not be reached for any steering transfer impedance A_2^{12}, so the steering designer may neglect these frequency ranges all together.

4.3.2. Target Achievement by Modified Front Axle Dynamics

Analogous to the preceding section, where steering modifications are proposed to meet vehicle targets, it is feasible to solve target deviations at vehicle level by modifications of the front axle subsystem. Additionally to the predicted global system dynamics assembled from actually found four-pole coefficients (black solid), Fig. 13 again contains expected vehicle performances based on *limiting curves* instead of *actual dynamics* of the front axle subsystem. In the case shown here, limiting curves to the axle force transmission ratio A_1^{11} are

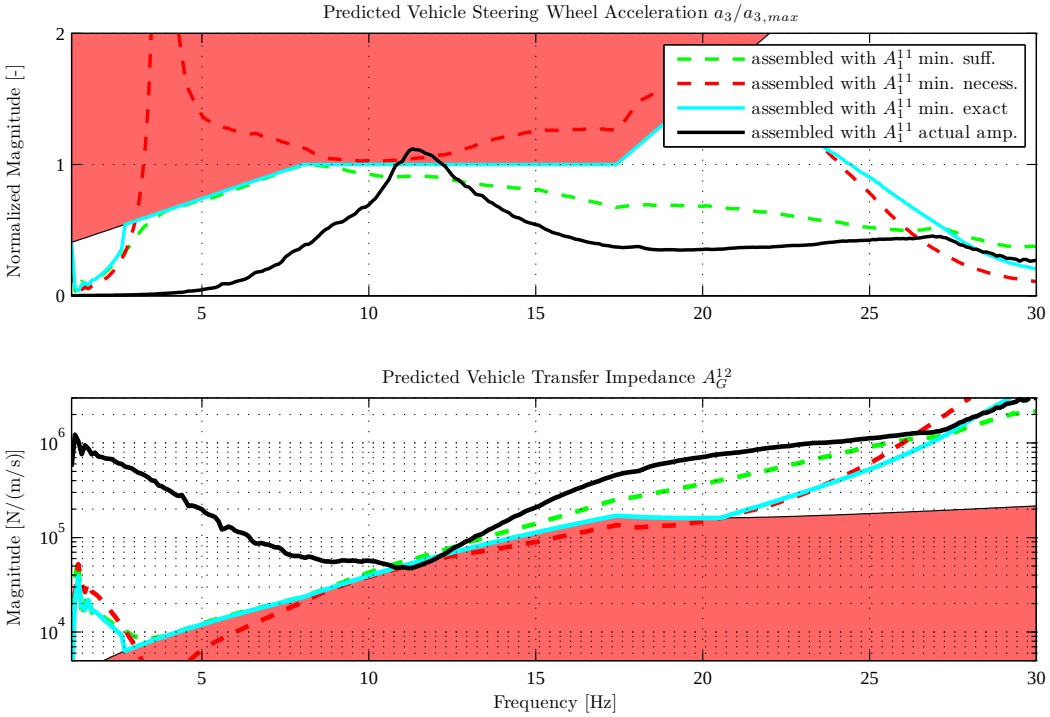

Figure 13: Vehicle Performance based on different Front Axle Dynamics compared to Vehicle Targets acc. to VDI2057 [14]

used for assembling, as derived in Section 4.2, whilst the axle transfer impedance and the steering four-pole coefficients are taken from actual testing or simulation results. Thus the vehicle transfer impedance A_G^{12} as well as the steering wheel vibration amplitudes a_3 are calculable with Eq. 18 and Eq. 15 respectively. The predictive results using the *exact limit* (cyan), the *sufficient limit* (green dashed) or the *necessary limit* (red dashed) to $A_1^{11}$are exactly the same as shown before in Section 4.3.1 at the example of steering modifications. This can be explained by Eq. 18, wherein the modified subsystem four-pole coefficients A_1^{11} and A_2^{12} represent the same component of the mathematical expression. Yet, the same results arise from different measures, either from modifications of the steering subsystem or from modifications of the front axle subsystem. This fact offers multiple ways to solve potential target deviation by subsystem modification. Which one of them will be preferred in practice depends on how easy design changes of the involved subsystem are realizable and if other, maybe conflicting, objectives are potentially violated.

5. Conclusion

This paper presents the application of substructuring to top-down vehicle steering design on the example of disturbing steering vibration. As the main focus is set on the decoupling of the subsystems involved, in order to derive requirements to the subsystem dynamics, the four-pole method is chosen. This method is considered to be the simplest substructuring technique with the lowest number of elements to be identified or specified, which is beneficial to apply substructuring to requirement derivation.

First of all, the vehicle as global system is divided into steering and front axle subsystems. Basic equations are derived in order to determine the needed elements of the four-pole matrices and their assembling and disassembling respectively. Requirements in terms of necessary, sufficient and phase-exact limit values to selected subsystem dynamics are calculated. Then, vehicle targets are introduced, which can be expressed over vehicle speed or excitation frequency. Both virtual and experimental methods are shown to identify the needed four-pole coefficients of the steering and the front axle during the design and verification stages.

Chapter 4 applies the method to derive requirements to the steering and the front axle alternately. Necessary and sufficient limits to the dynamics of one of the subsystems can be defined, even if the phase angles are unknown. More precise limits can be defined if the phase angles are obtained during the analysis. The method can be used in practice, either considering that some four-pole coefficients of the subsystem of interest are constant or considering mutual changes of all four-pole coefficients of the subsystem to be designed. By assembling actual and permissible dynamics of the subsystems, depending on whether they are known exactly or just specified by lower and upper limits, the performance at vehicle level is pedictable. It is shown that target mismatch can be detected already at subsystem level during the design phase, where corrective measures are still feasible. Reversely, vehicle targets are met if the subsystems fulfill their respective requirements derived with the four-pole method.

Future work may focus on applying the method to systems with non-linear behavior whilst this paper concentrates on linear systems. Furthermore, the approach shown on the example of only two subsystems could be extended to higher number of subsystems and higher number of degrees of freedom at the driving points and their internal interfaces. For arbitrary structures where the subsystems are connected strongly neither in a parallel nor in a serial manner, the approach could be transferred to the more general methods of frequency based substructuring.

6. References

[1] B. Jetmundsen, R. L. Bielawa, W. G. Flannelly, Generalized Frequency Domain Substructure Synthesis, Journal of the American Helicopter Society 33 (1) (1988) 55–64.

[2] D. de Klerk, D. Rixen, S. Voormeeren, General Framework for Dynamic Substructuring: History, Review and Classification of Techniques, AIAA Journal 46 (5) (2008) 1169–1181.

[3] M. van der Seijs, D. de Klerk, D. Rixen, S. Rahimi, Validation of Current State Frequency Based Substructuring Technology for the Characterisation of Steering Gear–Vehicle Interaction, in: M. Allen, R. Mayes, D. Rixen (Eds.), Topics in Experimental Dynamic Substructuring, Proceedings of the 31st IMAC, A Conference on Structural Dynamics, 2013, Vol. 2, Springer International Publishing, New York, 2014, pp. 253–266.

[4] M. van der Seijs, E. Pasma, D. de Klerk, D. Rixen, A Comparison of Two Component TPA Approaches for Steering Gear Noise Prediction, in: M. Allen, R. Mayes, D. Rixen (Eds.), Dynamics of Coupled Structures, Proceedings of the 33rd IMAC, A Conference and Exposition on Structural Dynamics, 2015, Chapter: 7, Vol. 4, Springer International Publishing, New York, 2015, pp. 71–79.

[5] M. Muenster, M. Lehner, D. Rixen, Requirements for the Disturbance Response of Steering and Suspension Systems based on Vehicle Targets, in: 14th International Stuttgart Symposium, Stuttgart, 2014, pp. 861–878.

[6] M. Muenster, M. Lehner, D. Rixen, M. Zimmermann, Vehicle Steering Design Using Solution Spaces for Decoupled Dynamical Subsystems, in: P. Sas, D. Moens, H. Denayer (Eds.), Proceedings of the International Conference on Noise and Vibration Engineering ISMA 2014, KU Leuven, Leuven, Belgium, 2014, pp. 3891–3905.

[7] C. T. Molloy, Use of Four-Pole Parameters in Vibration Calculations, The Journal of the Acoustical Society of America 29 (7) (1957) 842.

[8] J. Snowdon, Mechanical Four-Pole Parameters and their Application, Journal of Sound and Vibration 15 (3) (1971) 307–323.

[9] J. Y. Ha, K. J. Kim, S. Jung, Experimental Analysis of the Vibrations of Car Body and Steering Wheel System of a Passenger Car Using the Four-Pole Parameter Method, Machine Vibration 1 (3) (1992) 190–196.

[10] J. Y. Ha, K. J. Kim, Analysis of Mimo Mechanical Systems Using the Vectorial Four-Pole Parameter Method, Journal of Sound and Vibration 180 (2) (1995) 333 – 350.

[11] T. Wu, P. Zhang, C. Cheng, Boundary Element Analysis of Mufflers with an Improved Method for Deriving the Four-Pole Parameters, Journal of Sound and Vibration 217 (4) (1998) 767–779.

[12] J. Dickens, Methods to Measure the Four-Pole Parameters of Vibration Isolators, Acoustics Australia 28 (1) (2000) 15–21.

[13] H. Sell, Charakterisierung des dynamischen Verhaltens von elastischen Bauteilen im Einbauzustand, Ph.D. thesis, Technische Universitaet Hamburg-Harburg (2005).

[14] VDI 2057-2:2002, Part 2: Human Exposure to Mechanical Vibration, Association of German Engineers (VDI), 2002.

[15] ISO 5349-2:2001 Mechanical Vibration, Part 2: Measurement and Evaluation to Human Exposure to Hand-Transmitted Vibration, International Organization for Standardization (ISO), 2001.

[16] M. Muenster, R. Bosbach, Virtual Roller Test Rig for Dynamic Suspension Analysis, in: MSC Software Global Vehicle Dynamics Conference 2016), Munich, Germany, 2016.

[17] C. Wimmer, M. Lehner, Investigations on Disturbance Transfer Behavior of Electric Power Steering, in: 1. Internationales Muenchener Fahrwerk-Symposium, Muenchen, 2009, pp. 311–323.

[18] C. Wimmer, Modellbasierte Entwicklung elektromechanischer Lenkungen, Ph.D. thesis, Technische Universitaet Kaiserslautern (2013).

[19] P. Pfeffer, M. Harrer, Steering Handbook, Springer International Publishing, Cham, Switzerland, 2017, Ch. Layout of Steering Systems, pp. 169–189.

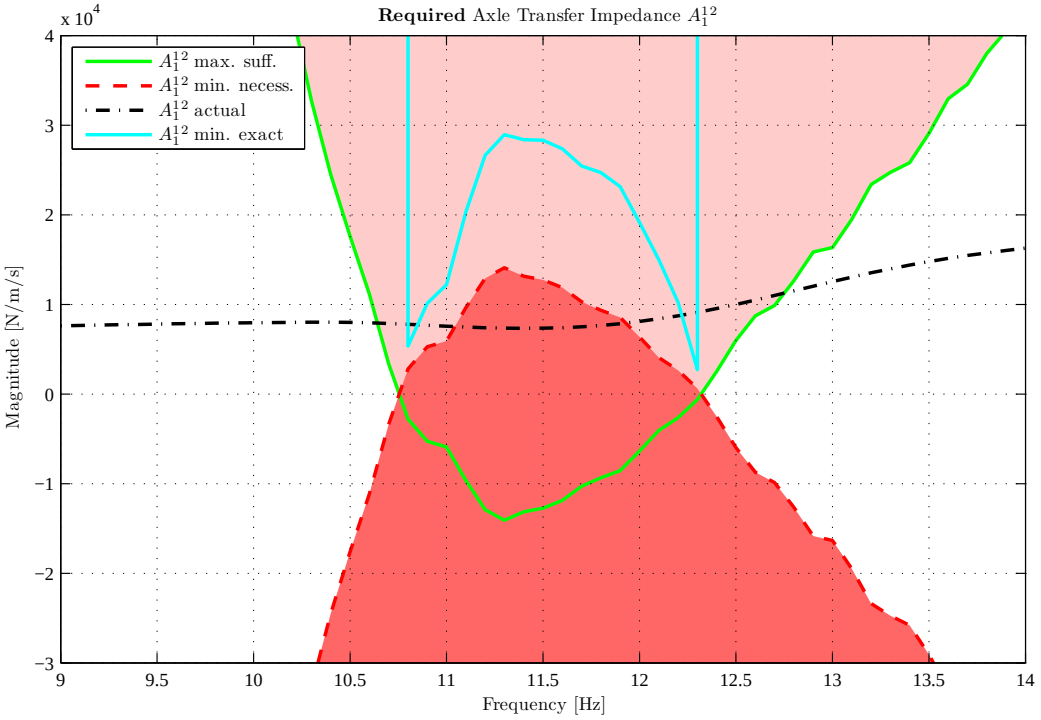

Figure A.14: Limiting curves to transfer impedance of the front axle in detail view

AppendixA. Graphical Interpretation of Limiting Curves

At first glance, the run of the limiting curves to the transfer impedance A_1^{12}, presented in Fig. 10 (upper right) and shown in detail in Fig. A.14, is not very comprehensible. For most frequencies, both the necessary and the exact, i. e. phase angle dependent, limits to the transfer impedance are far from the actual amplitude. But for some frequencies starting from about 10 Hz, the exact limit drops down very close to the actual amplitude while the necessary limit curve suddenly emerges from below. On the contrary the sufficient limit curve even dives into negative numbers. To understand these anomalies, it helps to visualize the phase-angle dependent composition of the subsystem dynamics with reference to the vehicle target using argand diagrams as schematically introduced in Fig. 3. According to Eq. 23 and Eq. 24, the subsystem dynamics can be displayed as complex numbers z_1 and z_2, where the transfer impedance A_1^{12} is part of z_2. Fig. A.15 visualizes the assembly of actual steering and front axle four-pole coefficients at chosen frequencies of $10,5$ Hz and $11,5$ Hz, which represent two different cases:

1. At $10,5$ Hz, shown in the left chart of Fig. A.15, the magnitude of z_1 is higher for all phase angles (green circular area) than the required magnitude of the assembly (magenta circle), representing the vehicle target. At the same time the magnitude of z_2 is comparatively small, so that it is impossible for any phase angle to end up with a lower magnitude of the assembly than required. Additionally, the actual phase angle of z_2 with respect to z_1 points away from the circle of minimum required magnitudes (magenta). In other words there are no requirements to the phase-exact limit at this frequency.

   For the necessary limit under in-phase alignment of z_1 and z_2, which effectuates the elongation of the resultant, no positive values can be calculated either.

   Regarding the sufficient limit under anti-phase alignment of z_1 and z_2, which produces shorter resultant compared to z_1, the distance from the arrowhead of $z_1$to the circle of minimum magnitudes (magenta) is of relevance. That distance quantifies the maximum permissible magnitude of z_2, which is affected by the transfer impedance A_1^{12} of the front axle.

2. The other case occurs at $11,5\,\mathrm{Hz}$, shown in the right chart of Fig. A.15, where the sum of z_1 and z_2 is always lower than the minimum required magnitude of the assembly. As indicated by the circular area (green), the required magnitude cannot be reached for any phase angle. Now, a minimum required phase-exact magnitude to z_2 and thus to the transfer impedance can be quantified, as indicated by the cyan arrow starting from z_1 and ending at the circle of minimum required magnitudes of the assembly.

   Similarly, for the necessary limit under in-phase alignment, the shortest distance from z_1 to the circle of minimum required magnitude of the assembly represents the minimum required magnitude to z_2.

   Regarding the sufficient limit under anti-phase alignment, some negative values of the magnitude of z_2 would lead to the required minimum magnitude of the assembly. Alternatively, very large positive values (more than twice as large as z_1) would cross the circle of minimum required magnitude of the assembly on the opposite side. But in fact, both of these options are not practicable at all.

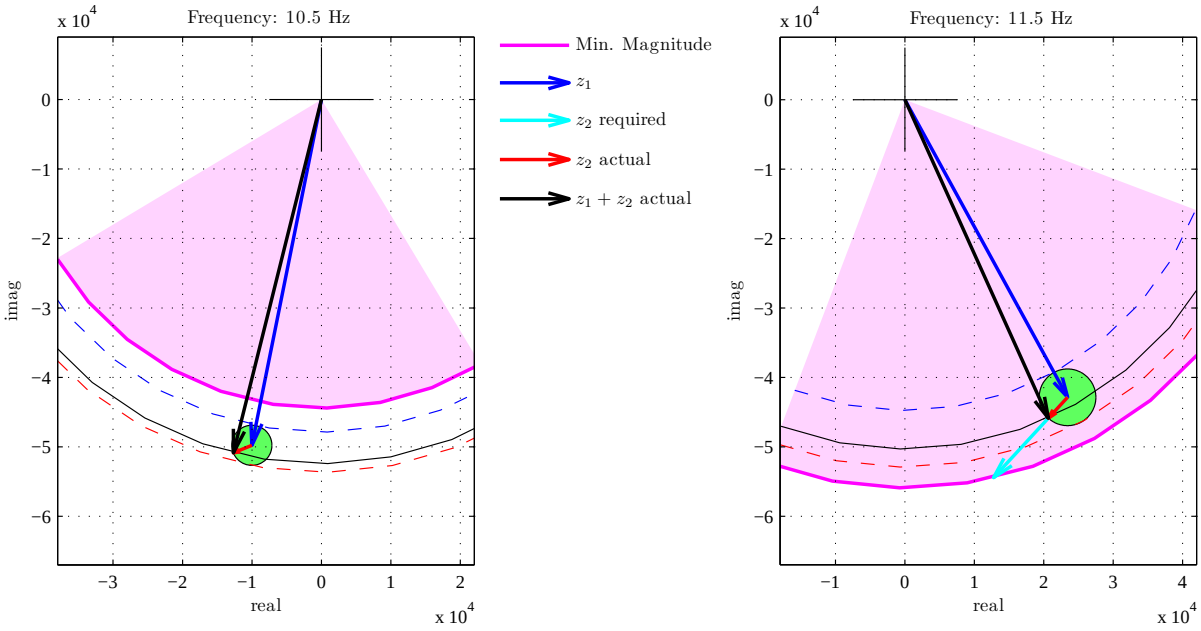

Figure A.15: Argand Diagram of the composition of front axle and steering dynamics